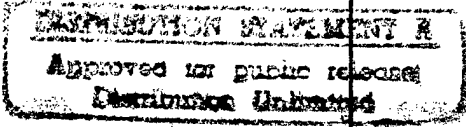


REPORT DOCUMENTATION PAGE			Form Approved OMB No. 0704-0188	
Public reporting burden for this collection of information is estimated to average 1 hour per response, including the time for reviewing instructions, searching existing data sources, gathering and maintaining the data needed, and completing and reviewing the collection of information. Send comments regarding this burden estimate or any other aspect of this collection of information, including suggestions for reducing this burden, to Washington Headquarters Services, Directorate for Information Operations and Reports, 1215 Jefferson Davis Highway, Suite 1204, Arlington, VA 22202-4302, and to the Office of Management and Budget, Paperwork Reduction Project (0704-0188), Washington, DC 20503.				
1. AGENCY USE ONLY (Leave blank)		2. REPORT DATE 1996		3. REPORT TYPE AND DATES COVERED Interim
4. TITLE AND SUBTITLE LIDAR Remote Sensing of Sound Velocity in the Ocean			5. FUNDING NUMBERS G N00014-96-1-0410	
6. AUTHOR(S) Edward S. Fry				
7. PERFORMING ORGANIZATION NAME(S) AND ADDRESS(ES) Texas A&M Research Foundation Box 3578 College Station, TX 77843			8. PERFORMING ORGANIZATION REPORT NUMBER 3249	
9. SPONSORING/MONITORING AGENCY NAME(S) AND ADDRESS(ES) Office of Naval Research Ballston Centre Tower One 800 North Quincy Street Arlington, VA 22217-5660			10. SPONSORING/MONITORING AGENCY REPORT NUMBER	
11. SUPPLEMENTARY NOTES				
12a. DISTRIBUTION / AVAILABILITY STATEMENT Approved for Public Release			12b. DISTRIBUTION CODE	
				
13. ABSTRACT (Maximum 200 words) <p>The project is progressing very well, and the first sound-velocity measurement using our non-scanning technique should be performed by summer 1997. No major problems have been encountered during the first year of this project. Several improvements of the experimental set up, and new possibilities are being considered: (1) Faraday Anomalous Dispersion Optical Filters (FADOF) using an excited state of Potassium could be also used as edges filters and their use is under study. It will have the advantage of rejecting background noise and having a very high transmission. (2) The width of the Brillouin lines is due to acoustic damping (absorption). By measuring this linewidth we can obtain data on the loss mechanisms - specifically bulk viscosity and shear viscosity. There is presently no experimental data for water on the former. An experimental set up similar to the one for Brillouin frequency shift measurement could serve this measurement.</p>				
			19970210 045	
14. SUBJECT TERMS			15. NUMBER OF PAGES	
			16. PRICE CODE	
17. SECURITY CLASSIFICATION OF REPORT UNCLASSIFIED	18. SECURITY CLASSIFICATION OF THIS PAGE UNCLASSIFIED	19. SECURITY CLASSIFICATION OF ABSTRACT UNCLASSIFIED	20. LIMITATION OF ABSTRACT UL	

LIDAR Remote sensing of Sound Velocity in the Ocean

Technical report (RF-3249)

1. Introduction:

Both Raman and Brillouin scattering can be considered for sound velocity measurements in the ocean using LIDAR. Previous experimental efforts have concentrated on Raman scattering. The broad linewidth of Raman radiation (about 15 nm) does not permit good background noise and fluorescence rejection, and measurements have not shown the required accuracy. While they have similar cross sections, $1.5 \cdot 10^{-4} \text{ m}^{-1} \text{ sr}^{-1}$ for Raman, $2.4 \cdot 10^{-4} \text{ m}^{-1} \text{ sr}^{-1}$ for Brillouin, the Brillouin lines have the advantage that their linewidth is only 0.5 GHz. A proper design of the receiver makes a system based on this scattering process insensitive to background radiation and provide accurate measurements. Typical Brillouin shifts are between 7 and 8 GHz, and a sensitivity of the order of a MHz is needed (i.e. 1 part in 500 of Brillouin line).

To demonstrate a Brillouin LIDAR system, the first year's work has been in two directions: (1) analysis of the limitation on the accuracy of the sound velocity retrieval using Brillouin scattering, and (2) development of the Brillouin LIDAR receiver using the edges of Br₂ and I₂ absorption lines. The progresses for each part are described in Sect 2 and 3 respectively.

2. Sound velocity determination

As a baseline for the discussion, we consider an airborne LIDAR, operating at 532 nm, with a energy of 500 mJ/pulse, single pulse measurement, and a depth resolution of 1.1 m. Accuracy of the measurement could be increased by averaging over several shots, decreasing the depth resolution, or decreasing the LIDAR total range by using the system on a boat, submarine, or buoy. Depending on the depth and the hydrosol content of the ocean water, the standard deviation Δv_B on the Brillouin shift measurement range between 0.5 and 4 MHz [Hickman et. al., 1991].

We have made the first rigorous analysis of the accuracy of sound velocity measurements using a Brillouin LIDAR. Previous studies were very incomplete and frequently misleading (Guagliardo et. al., 1980; Hirschberg and Dufilho, 1984; Leonard and Sweeney 1988; and Hickman et. al., 1991). To determine the sound velocity from the Brillouin shift measurement, there are five parameters (Salinity, Temperature, Sound velocity, Refractive index, and Brillouin shift); past studies identify, in the best case, only four relationships among them. To solve the system of equations, by providing a fifth relationship, we have analyzed the historical salinity measurements provided by the data set of

the Oceanographic Station time Series compiled by the national Oceanographic Data Center (NODC). More than 75,000 data have been analyzed to determine the knowledge in the salinity mean value and standard deviation for a given location and for a given depth. The important result about that is that for a given depth and location, the salinity standard deviation is small and will enable us to retrieve sound velocity with an accuracy better than 1 m/s for all locations. Such an accuracy is sufficient for numerous applications. A summary of our results for sound velocity error as a function of the salinity standard deviation ΔS for various measurements of the Brillouin shift accuracy Δv_B is shown in Fig. 1; a salinity standard deviation histogram is superimposed on it. A paper describing these results has been submitted to Applied Optics. A copy of it is attached to this report.

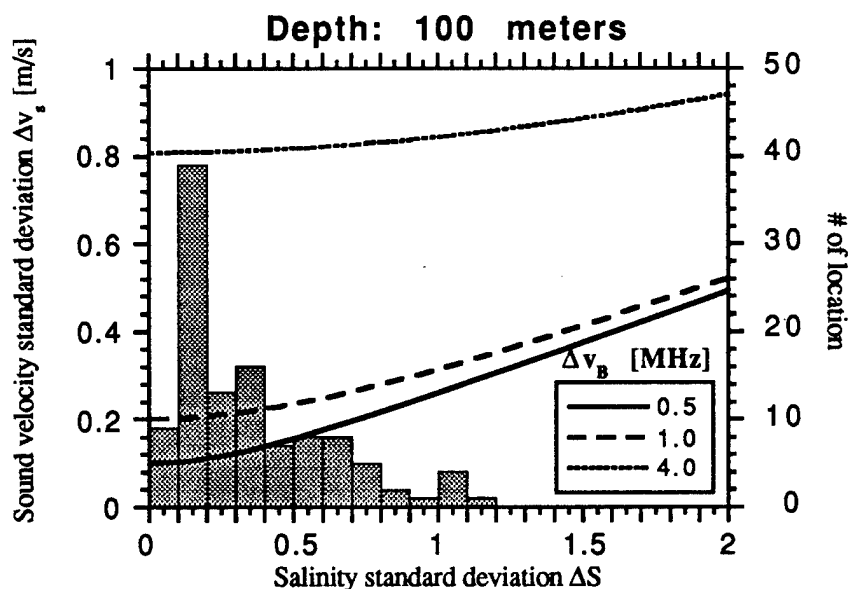


Fig 1. Sound velocity standard deviation as a function of the Salinity standard deviation superposed with the salinity standard deviation histogram. computed from Ref. 7.

The standard deviation of the Salinity-Temperature (S-T) relationship was also examined using the data set of the NODC. Some typical plots of the salinity (in ‰) as a function of the temperature (in °C) are shown in Fig. 2 and 3. The mean value of the salinity is represented by a solid line, and the standard deviation with dotted lines. The diamond-shaped points represent the measured pairs (T,S). As can be seen in Fig. 2, we have found a clear correlation between salinity and temperature for a few locations, generally for large depths. Nevertheless, the general case, in particular for the upper-ocean mixed layers, is almost always represented by Fig. 3 which shows no correlation. For our application, this means that for some locations only, the precision of the measurement could be increased by considering the S-T relationship.

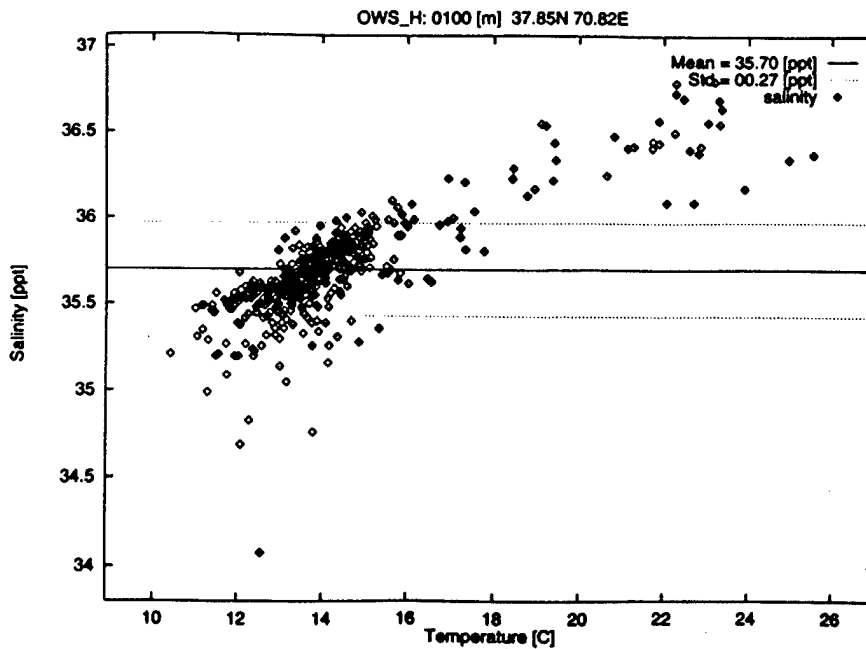


Fig 2 Mean value (solid line) and standard deviation (doted lines) of the salinity, and pairs (T,S) computed from Ref. 7 (diamond-shaped points) for the location 37.85N, 70.82E. at a depth of 100 m. Notice the correlation between the salinity and the temperature.

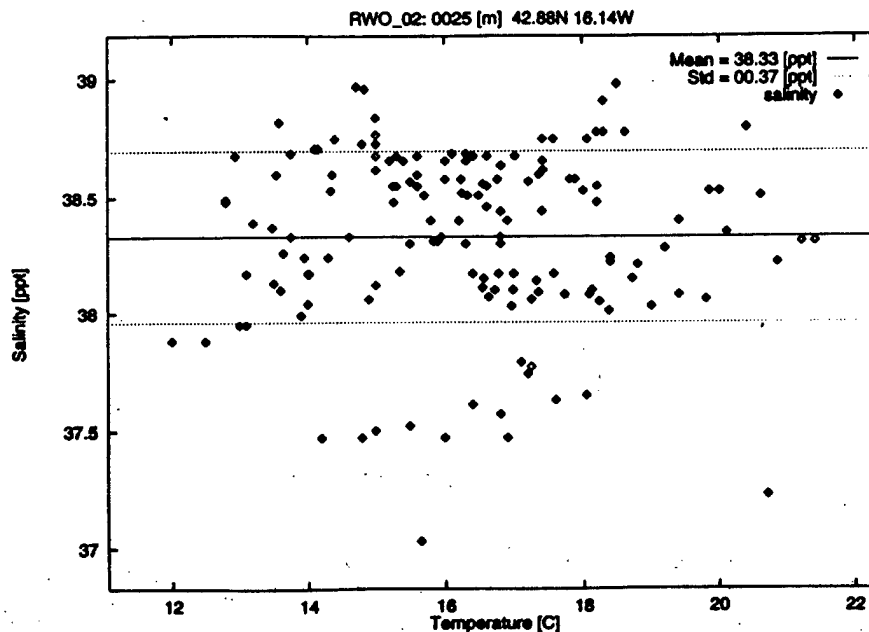


Fig 3 Mean value (solid line) and standard deviation (doted lines) of the salinity, and pairs (T,S) computed from Ref. 7 (diamond-shaped points) for the location 62.00N, 33.27E. at a depth of 25 m. There is no correlation between the salinity and the temperature.

3. Brillouin shift measurement

The typical Brillouin shift sensitivity to be expected is of the order of a MHz. For LIDAR measurements the anticipated parameters are a depth resolution of 1.1 m (which requires a 10 ns laser pulse), and a 0.1 GHz data acquisition rate. The technical requirements are: (1) a stabilized Fourier transform limited bandwidth pulse laser; and (2) a non scanning spectroscopic method for Brillouin shift discrimination.

In preliminary work to be used as a reference for our work we have used a Fabry-Perot interferometer to make the first experimental frequency resolved measurements of the Brillouin lines with a pulsed laser at high resolution. Fig. 4 shows a measured frequency spectrum, superposed on the theoretical one for a water temperature of 29°C (corresponding to a Brillouin shift of 7.55 GHz). Only one free spectral range of the Fabry-Perot is presented in the figure. The experimental points are raw data from a single scan; no further processing has been performed. There is very good agreement with theory. The strong central peak is due to particulate contamination of the water. Prior to these results, no frequency resolved measurements using a pulsed laser had been made. The only available previous results did not demonstrate sufficient frequency resolution due to laser linewidth and probably poor collimation through the Fabry-Perot frequency analyzer. [Guagliardo et. al., 1980].

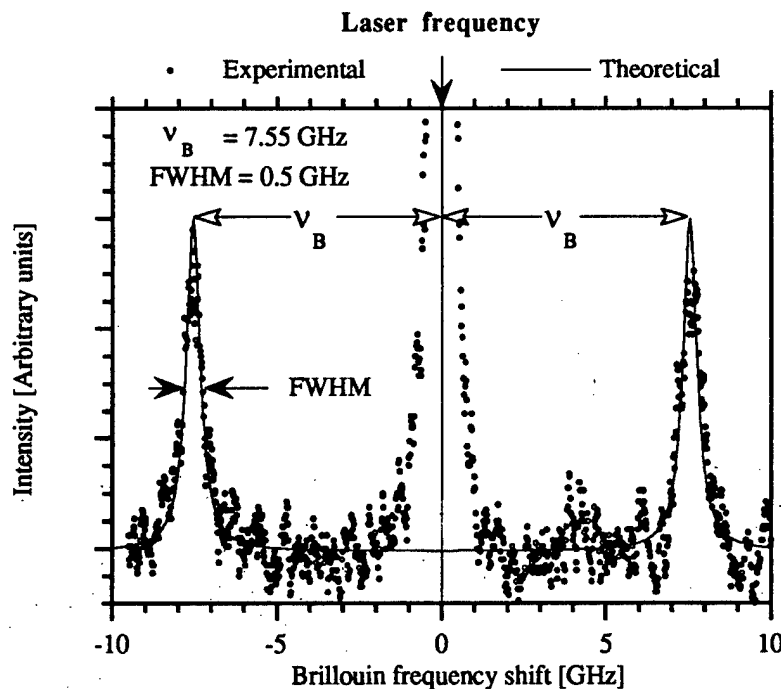


Fig 4. Experimental (dots) and theoretical Brillouin spectrum of water at 29 °C using the second harmonic of a pulsed injection seeded Nd:YAG laser (532 nm).

These measurements and the experimental set up have been presented in the Ocean Optics XIII conference in Halifax, and have been published in the SPIE conference proceedings. A copy is attached to this report. These results using a scanning measurement technique demonstrate that the stability of the laser is not a limiting factor for the measurement of the Brillouin frequency shift using a LIDAR instrument, the results also provide an essential tool for the next tasks of the project. For application to Brillouin LIDAR measurements, we require a better accuracy (the scanning Fabry-Perot technique will not provide a measurement accuracy of 1/500 the Brillouin linewidth) and a non scanning method (due to LIDAR timing requirement).

The edge technique used in conjunction with Br₂ and I₂ absorption cells will serve these requirements. Explicitly, the frequency of the laser transmitter is chosen so that the edges of two different molecular absorption lines (with opposite slopes) are located at the centers of the Brillouin lines. Because of the steep slope of the absorption edges, small changes in the Brillouin shift produce large changes in transmission. A more precise description of the experimental set up is given in the proceeding of the Halifax conference attached to this report. For this spectroscopic purpose, we succeeded in obtaining second harmonic generation (1064 nm to 532 nm) for measuring the I₂ and Br₂ spectra and for locking the frequency of the seed laser used to injection lock the pulsed Nd:Yag laser. A nice feature is that our new method does not require stabilization of the doubling crystal temperature, contrary to past approaches which required stabilization of the crystal to a few millidegrees. The spectroscopic set up is now ready. The Br₂ cells should be ready for the end of the year, and the ¹²⁹I₂ cell should arrive soon from China.

3. Summary

The project is progressing very well, and the first sound-velocity measurement using our non-scanning technique should be performed by the summer 1997. No major problems have been encountered during the first year of this project. Several improvements of the experimental set up, and new possibilities are being considered:

- Faraday Anomalous Dispersion Optical Filters (FADOF) using an excited state of Potassium could be also used as edges filters and their use is under study. It will have the advantage of rejecting background noise and having a very high transmission.
- The width of the Brillouin lines is due to acoustic damping (absorption). By measuring this linewidth we can obtain data on the loss mechanisms - specifically bulk viscosity and shear viscosity. There is presently no experimental data for water on the former. An experimental set up similar to the one for Brillouin frequency shift measurement could serve this measurement.

Since this project is so closely involved with physical oceanography, the graduate student in this project, Jeffery Katz, has enrolled in a course in graduate level physical oceanography this semester.

5. References

1. G.D. Hickman, J.M. Harding, M. Carnes, A. Pressman, G.W. Kattawar, and E.S. Fry, "Aircraft Laser Sensing of Sound Velocity in Water: Brillouin Scattering," *Remote Sens. Environ.* 36, 165-178 (1991).
2. D.J. Collins, J.A. Bell, R. Zanoni, I.S. McDermid, J.B. Breckinridge, and C.A. Sepulveda, "Recent Progress in the Measurement of Temperature and Salinity by Optical Scattering," in *Ocean Optics VII*, M.A. Blizard, ed., *Proc. SPIE* 489, 247-269 (1984).
3. D.A. Leonard and H.E. Sweeney, "Remote sensing of ocean physical properties: a comparison of Raman and Brillouin techniques" *SPIE Vol. 925 Ocean Optics IX* 1988.
4. D.A. Leonard and B. Caputo: "Remote sensing of the ocean mixed-layer depth" *Optical engineering* Vol 22(3) 1983
5. J.L. Guagliardo, H.L. Dufilho, "Range resolved Brillouin scattering using a pulsed laser" *Rev. Sci. Instrument.* 51(1) 1980
6. J.G. Hirschberg, J.D. Byrne, A.W. Wouter, and G.C. Boynton: " Speed of sound and temperature in the ocean by Brillouin scattering" *Applied Optics*, Vol 23(15) 1984
7. "Oceanographic Station Profile Time Series," National Oceanographic Data Center (NODC), User Services Branch, NOAA/NESDIS E/OC21, Washington, D.C., 1993.

Laboratory development of a LIDAR for measurement of sound velocity in the ocean using Brillouin scattering

Yves Emery and Edward S. Fry

Physics department, Texas A&M University, College Station, TX, USA, 77843-4242

Tel. (409) 845 19 10, Fax (409) 845 25 90, Email fry@phys.tamu.edu.

ABSTRACT

There have been several studies of the potential accuracy of LIDAR measurements of sound velocity in the ocean by measuring the spectral shift of the backscattered Brillouin lines. However, due to technical limitations, such systems have not previously been experimentally demonstrated. Measurement of the Brillouin shift as a function of depth in the ocean requires a stabilized, narrow linewidth, pulsed laser, and a high-resolution spectroscopic technique. We have used a scanning Fabry-Perot to obtain the first frequency resolved measurements of Brillouin scattering in water using a pulsed laser; these results will be presented here. But for the practical application of measuring Brillouin shifts as a function of depth in the ocean a non-scanning spectroscopic technique is required to measure the small frequency shifts; the edge technique meets this requirement. Using it in conjunction with the edges of absorption lines in the molecular spectra of I_2 and/or Br_2 , avoids the limitations associated with use of a Fabry-Perot etalon; specifically, its small solid angle of acceptance and its vulnerability in noisy environments. This new approach will be briefly described.

Keywords: Brillouin LIDAR remote sensing, sound velocity, ocean, edge technique, molecular absorption lines.

1. INTRODUCTION

Several studies have discussed the importance of remote measurements of sound velocity in the upper-ocean mixed layer.¹⁻⁵ Real-time range-resolved monitoring provides a crucial input to the understanding of the physical behavior of the ocean. A Brillouin LIDAR is a promising tool for such remote measurements of the sound velocity as a function of depth. Brillouin scattering produces two inelastically scattered Lorentzians centered symmetrically with respect to the laser line; they have a FWHM of about 0.5 GHz. The so-called Brillouin shift v_B , that is to say the frequency shift between the laser line and each of the Brillouin lines, is typically between 7 and 8 GHz, and is proportional to the sound velocity. In pure water, the scattering spectrum is almost solely composed this doublet. An elastically scattered central line (also called the unshifted line, or improperly the Rayleigh line)⁶ appears when the water is contaminated by hydrosols.

The limits in the accuracy of sound velocity and temperature profiles in the ocean from LIDAR Brillouin shift measurements have been discussed in detail by Fry, *et al.*⁷ Briefly, for a given incident laser wavelength λ the Brillouin shift v_B is proportional to the refractive index of water n and the sound velocity v_s . The refractive index itself is function of the salinity S and temperature T . In addition to these two variables, the sound velocity also has a weak dependence on pressure, but for present purposes, this dependence will be neglected; the generalization to include pressure dependence is straightforward. The Brillouin shift is then expressed as:

$$v_B(S, T) = \frac{2n(S, T)}{\lambda} v_s(S, T) \sin(\theta/2), \quad (1)$$

where θ is the scattering angle ($\sin(\theta/2)=1$ for 180° backscattering). Clearly, there are five parameters (v_B , v_s , n , S , and T), but there are only three relations between them and only one measurement (v_B). The three relations are Eq. 1 and empirical equations for $n(S, T)$ and $v_s(S, T)$. Thus one additional piece of information is required. For present purposes, it is provided by the means and standard deviations of the extensive set of salinity measurements (from 1900 to 1990) compiled by the National Oceanic and Atmospheric Administration.⁸ With these salinity estimates based on historical data, i.e. without actual measurements of salinity, the limits on the sound velocity accuracy can be better than 0.3 m/s.

Our primary interest is in developing a LIDAR for range-resolved measurements of sound velocity in the ocean via the measurement of the Brillouin shift. Although the idea of a Brillouin LIDAR is not new,¹⁻³ such systems have not yet been experimentally demonstrated due to technical limitations. Measurements of the Brillouin shift as a function of depth in the ocean requires both a stabilized narrow linewidth pulsed laser, and a high-resolution non-scanning spectroscopic technique.

Sound velocity measurements with depth resolution δz of 1 meter require a Brillouin frequency shift measurement for each successive 10 ns ($=2\pi\delta z/c$) interval of the LIDAR return. In addition, a precision of 1 m/s for the sound velocity requires the measurement of Brillouin shifts with an accuracy better than about 4 MHz.⁷ This small value compared to the linewidth of the Brillouin line (500 MHz) does not allow the use of a conventional spectrometer. In this paper we discuss our recent progress in development of a Brillouin LIDAR.

The first laboratory measurements of frequency resolved Brillouin lines using a pulsed laser and a scanning Fabry-Perot technique for frequency discrimination are presented in Sect. 2. Previous pulsed laser measurements² were not completely resolved, but our results clearly demonstrate this resolution with pulsed lasers. However, the scanning Fabry-Perot measurement technique used to obtain this data is not accurate and fast enough to be used directly for LIDAR measurements of the Brillouin shift. Nevertheless, these results and the measurement apparatus will provide a valuable reference for the initial data obtained with our new non-scanning spectroscopic technique.

This new technique is a version of the edge technique, and is a powerful non-scanning spectroscopic technique for the measurement of small frequency shifts.⁹ It has numerous applications, and has been successfully used in a Doppler LIDAR for atmospheric wind velocity measurements.¹⁰ From the standpoint of an oceanic Brillouin LIDAR, the main limitations of previous implementations of this method are the small acceptance angle of the Fabry-Perot etalons used for the frequency discrimination, and the difficulties associated with operating these interferometers in noisy vibrational and acoustic environments. We are implementing a version of the edge technique in which the frequency discriminants are the edges of absorption lines in the molecular spectra of I_2 and/or Br_2 . Explicitly, the frequency of the laser transmitter is chosen so that the edges of two different molecular absorption lines (with opposite slopes) are located at the centers of the Brillouin lines. Because of the steep slope of the absorption edges, small changes in the Brillouin shift produce large changes in transmission. The details of the experimental set up are described in Sect. 3.

2. FREQUENCY RESOLVED MEASUREMENTS OF BRILLOUIN LINES

The theoretical model for Brillouin scattering in a liquid was developed by Mountain⁴ and Fabelinskii.¹¹ Early attempts to examine the use of Brillouin scattering for the determination of sound velocity in pure water were by Chiao, *et al.*¹² and by Benedek, *et al.*¹³ Since then, considerable effort with CW lasers has been reported,⁵ but no definitive results have previously been performed using a pulsed laser. To our knowledge, the only such published results show a FWHM of the Brillouin lines of about 3 GHz; this indicates that the stability and linewidth of the laser transmitter were not sufficient.²

Our experimental set up for the Brillouin spectrum measurements is shown in Fig. 1. A frequency doubled, injection seeded, Q-switched, pulsed Nd:YAG laser provides 75 mJ at 532 nm, with a repetition rate of 10Hz. Using an injection locking technique developed in our laboratory,¹⁴ it operates at a single frequency and has stable Fourier transform limited pulses of 10 ns, i.e. a frequency bandwidth of about 50 MHz. A horn shaped water cell is used to avoid backreflections. An additional light baffle consisting of two pierced parallel plates was added in the bottom of the water cell to further suppress parasitic backreflections. Noise due to the reflection from the surface of the water is avoided by using another thin baffle plate. The backscattered light is collected at an angle of 175° relative to the laser beam direction. The acceptance angle of the optical system is $\approx 1^\circ$ and is determined by the focal length and the size of lens L1; this acceptance angle does not significantly increase the FWHM of the Brillouin lines. The most critical point in order to obtain good frequency discrimination is to provide a very well collimated beam to the input of the Fabry-Perot (FP) etalon. A spatial filter consisting of 2 lenses (L1 and L2), a pinhole (P1) of 10 μ m diameter, and one iris (I) is used for this purpose. To avoid background radiation, the output of the etalon is focused through pinhole P2 onto a photomultiplier, PM, and the overall receiver system is enclosed in a black box.

The Fabry-Perot has a resolution of 0.25 GHz ($R=96\%$) and a Free Spectral Range (FSR) of 18 GHz. The etalon piezoelectric transducers are driven by a Burleigh RC-42 ramp generator. The measurements are performed with a scanning ramp duration of 2 minutes per FSR. The detector is a Hamamatsu R446 photomultiplier tube operating in the analog mode. The signal is integrated and averaged over 10 laser shots by a gated integrator and boxcar averager. It is digitized and stored using a Labview program on a MacII computer.

Fig. 2 shows a measured frequency spectrum, superposed on the theoretical one for a water temperature of 29°C (corresponding to a Brillouin shift of 7.55 GHz). Only one free spectral range of the Fabry-Perot is presented in the figure. The experimental points are raw data from a single scan; no further processing has been performed. There is very good

agreement with theory. The strong central peak is due to particulate contamination of the water, which is apparently due mostly to oxidation of the metal light baffle submerged in the horn shaped water cell.

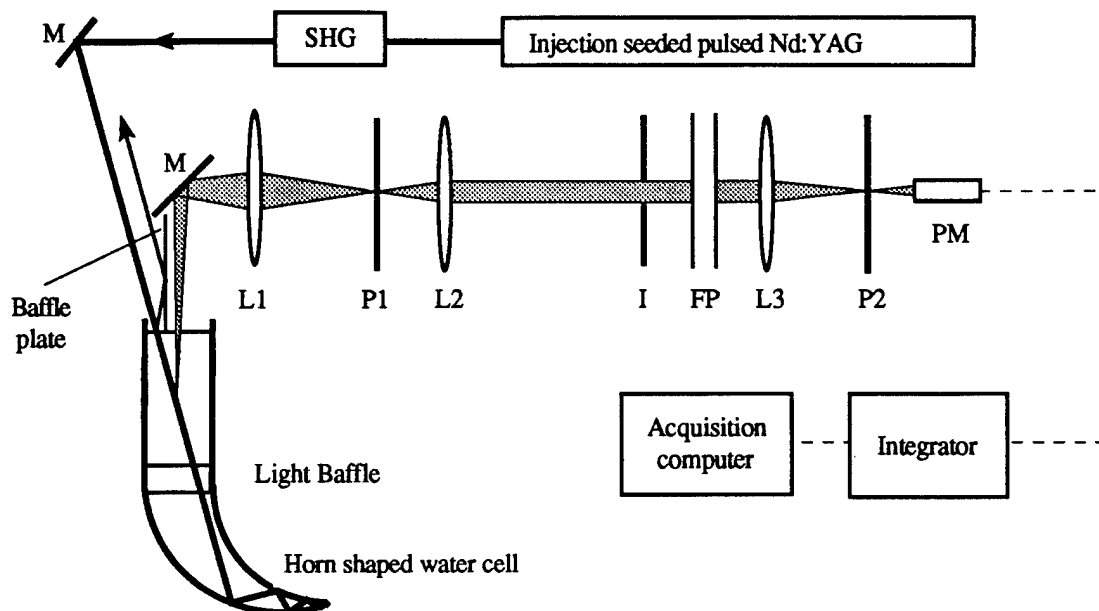


Fig. 1. Brillouin spectrum measurement set up. L1, L2, and L3 are biconvex lenses of focal length 50 cm, 20 cm and 8 cm, P1 is a 10 μm diameter pinhole, I is an iris used to select the lower interference order, P2 is a 1 mm diameter pinhole, SHG is second harmonic generator, M are mirrors, and PM is the photomultiplier.

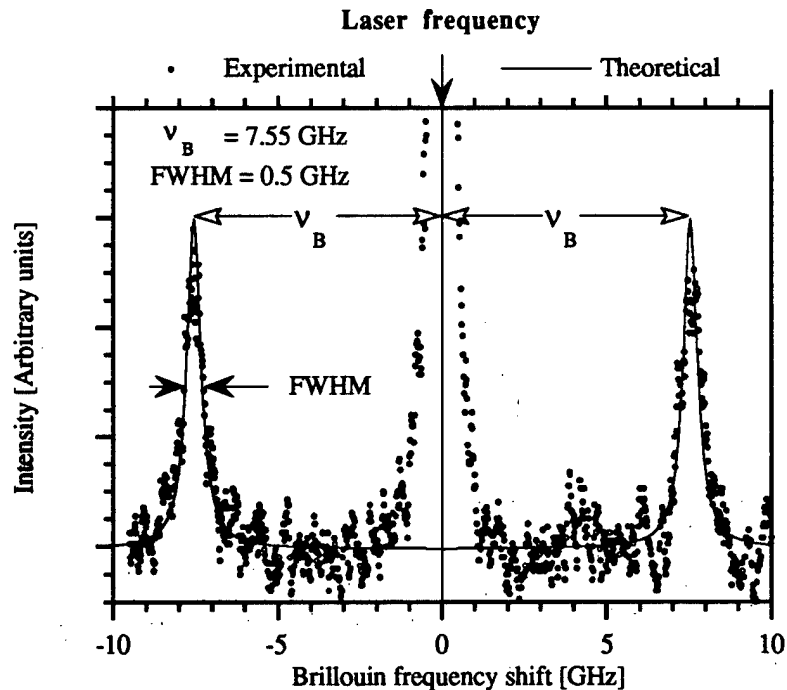


Fig. 2. Experimental (dots) and theoretical Brillouin spectrum of water at 29°C using the second harmonic of a pulsed injection seeded Nd:YAG laser (532 nm).

3. BRILLOUIN SHIFT MEASUREMENT

As discussed in the introduction, a Brillouin LIDAR based on a version of the edge technique is under development. Using the edge technique, atmospheric measurements at 1064 nm have shown wind velocity accuracies of 0.25 m/s, corresponding to frequency changes smaller than 470 kHz.¹⁰ This is the most sensitive method yet demonstrated for small frequency shift LIDAR measurements.¹⁵ Versions of the edge technique had already been considered by Hirschberg, *et al.*³ and by Hickman, *et al.*¹ for oceanic Brillouin shifts measurements using a laser wavelength of 532 nm. In the latter study the statistical uncertainty δv_B in the measurement of the Brillouin shift is calculated assuming a single laser shot with an energy of 500 mJ and a depth resolution of 1.1 meter. For $\gamma < 0.04 \text{ m}^{-1}$, shot noise limited uncertainties in δv_B of less than 1 MHz can be expected for depths down to 75 meters, and of less than 4 MHz down to 100 meters. These correspond to sound velocity measurement accuracies that can be better than 0.3 m/s and 1 m/s,⁷ respectively.

We are developing a version of the edge technique that makes use of the edges of absorption lines in the molecular spectra of I_2 and/or Br_2 , as opposed to the Fabry-Perot interferometers used in other applications^{1-3,9} of the edge technique. The schematic of such a LIDAR receiver is shown in Fig. 3. The second harmonic of an injection-seeded pulsed Nd:YAG laser is used as the transmitter. The laser signal backscattered by the ocean water is collected by a telescope, and is first directed through an atomic cell (used as a blocking-filter) where the central line of the backscattered frequency spectrum is absorbed. The backscattered signal transmitted by the blocking filter is then split into two equal parts: one part is detected to produce a normalization signal (S2). The other part passes through the edge filter and is detected to produce the signal (S1). The Nd:YAG laser frequency stabilization is performed by picking off a small part of the cw seed laser beam, frequency doubling it in an external ring build-up cavity, and locking the seed laser to the absorption line of the blocking-filter. The return signals S1 and S2 are sampled every 2-3 ns to produce a range-resolved measurement (of course, the temporal resolution is limited by the 10 nanosecond laser pulse).

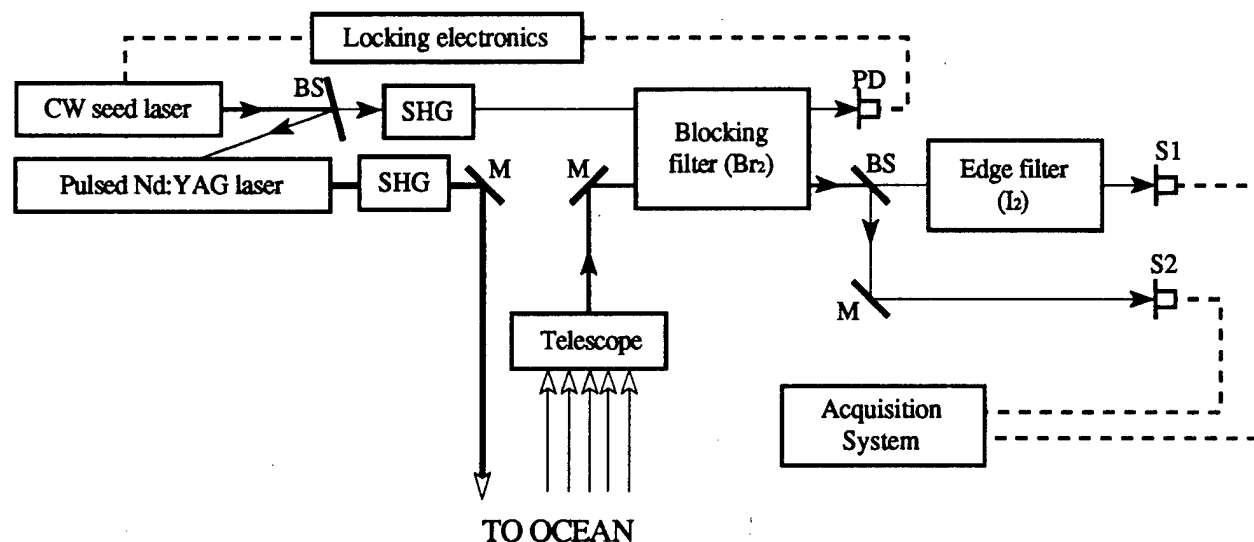


Fig. 3. Brillouin LIDAR receiver schematic. The Brillouin shift is determined from the ratio $S1/S2$. BS are beam splitters, M are mirrors, SHG is second harmonic generators, M are mirrors, and PD are photo detectors. Solid lines correspond to light paths, and dotted lines to electrical connections.

As an example of an edge filter, consider a $^{127}\text{I}_2$ absorption cell. For a laser wavelength of 532.573806 nm, it provides two appropriately positioned absorption edges (see Fig. 4). Because of the steep average slope of the absorption edges, small changes in the Brillouin shift produce large changes in the transmission of the edge filter. The temperature of the gas and/or the vapor pressure in the cells can be changed for a fine adjustment of the absorption line slopes and frequencies.

An important advantage of this edge filter version is that a change in the incident laser frequency or any Doppler shifts due to movements will increase the edge filter signal corresponding to one Brillouin line and decrease the signal corresponding to the other; thus such systematic effects are canceled to first order. The ratio $S1/S2$ provides a

normalization which makes the frequency discrimination independent of the intensity of the light backscattered by the ocean water, i.e. independent of the attenuation due to water absorption or hydrosols scattering.

An ideal blocking filter should exhibit total absorption for the central line of the backscattered spectrum, and good transmission for the Brillouin peaks. The FWHM of the central line is mainly the linewidth of the laser transmitter, and is ≈ 50 MHz. Fig. 5 shows the absorption spectrum of Br₂ superposed on theoretical Brillouin lines with a shift of 7.5 GHz, and for the same incident laser wavelength as for the I₂ data in Fig. 4. This absorption line provides a satisfactory, although not perfect blocking filter. Of course, the convolution of the Brillouin lines and of the transmission spectrum of Br₂ has to be considered as the input to the edge filter.

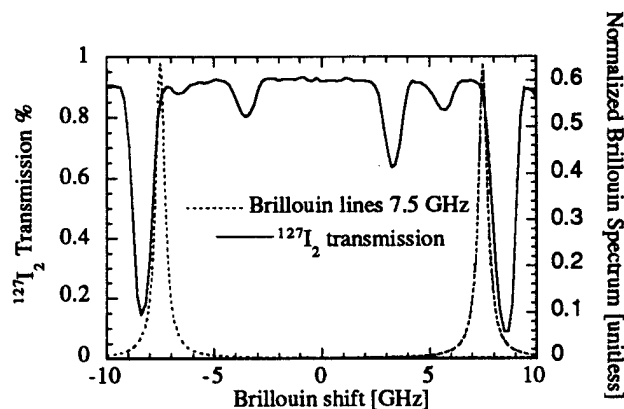


Fig. 4. Edge filter: theoretical Brillouin lines for a frequency shift of 7.5 GHz superposed on the absorption spectrum of $^{127}\text{I}_2$. Small changes of the Brillouin shift make large changes in the transmitted signal. The incident wavelength for the Brillouin spectrum is 532.573806 nm.

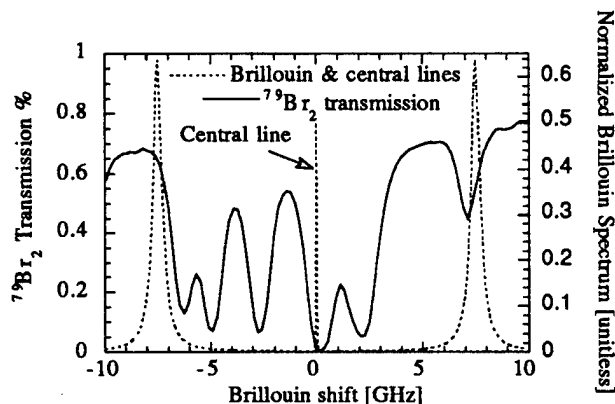


Fig. 5. Blocking filter : The ideal blocking filter should have a good transmission for the Brillouin lines and a total absorption for the central line of the backscattered spectrum. The absorption lines of $^{79}\text{Br}_2$ provide a satisfactory blocking filter for an incident laser wavelength of 532.573806 nm.

4. PROSPECTS AND CONCLUSION

We have shown that an injection seeded pulsed laser can be used to obtain completely resolved measurements of Brillouin lines. This verifies that Brillouin shift data can be used to measure sound velocity as a function of depth in the ocean. A version of the edge technique for the measurement of the Brillouin shift has been outlined.

In comparison to other LIDAR receiver designs (using, for example, a Fabry-Perot) the I₂ and/or Br₂ absorption cells provide a simpler and more robust approach that requires no critical alignments. The optical efficiency of a receiver using the absorption lines discussed here, would be as good as that using a Fabry-Perot based receiver. A systematic search for other combinations of transmitter wavelength and absorption lines is underway. This includes direct experimental examination and comparison of the absorption lines of $^{127}\text{I}_2$, $^{129}\text{I}_2$, $^{79}\text{Br}_2$, and $^{81}\text{Br}_2$.

5. ACKNOWLEDGMENTS

The authors would like to thank George Kattawar, Thomas Walther, Jeffery Katz, and Jason Pan for many useful discussions. The work is supported by the Robert A. Welch Foundation Grant No. A-1218, the Texas Advanced Technology Program Grant 010366-16, the Office of Naval Research Grant No N00014-96-1-0410, and the Swiss National Foundation of Sciences.

6. REFERENCES

1. G. D. Hickman, J. M. Harding, M. Carnes, A. Pressman, G. W. Kattawar, and E. S. Fry, "Aircraft Laser Sensing of Sound Velocity in Water: Brillouin Scattering", *Remote Sens. Environ.*, **36**, 165-178 (1991).
2. J. L. Guagliardo and H. L. Dufilho, "Range Resolved Brillouin Scattering Using a Pulsed Laser", *Rev. Sci. Instrum.*, **51**, 79-81 (1980).
3. J. G. Hirschberg, J. D. Byrne, A. W. Wouters, and G. C. Boynton, "Speed of Sound and Temperature in the Ocean by Brillouin Scattering", *Appl. Opt.*, **23**, 15, 2624-2628 (1984).
4. D. A. Leonard and B. Caputo, "Remote sensing of the ocean mixed-layer depth", *Optical Engineering*, **22**, 3, 288-91 (1983).
5. D. J. Collins, J. A. Bell, R. Zaoni, I. S. McDermid, J. B. Breckinridge, and C. A. Sepulveda, "Recent Progress in the Measurement of Temperature and Salinity by Optical Scattering", M. A. Blizards, *Ocean Optics VII*, vol. 489, pp. 247-263, (Proc. SPIE, 1984).
6. A. T. Young, "Rayleigh Scattering", *Physics Today*, **35**, 1, 42-48 (1982).
7. E. S. Fry, Y. Emery, X. Quan, and J. Katz, "On Brillouin LIDAR Measurements of Oceanic Temperature and Sound velocity", *Submitted to Applied Optics*, (1996).
8. National Oceanographic Data Center (NODC), User Services Branch, NOAA/NESDIS E/OC21, Washington, D. C., (1993).
9. C. L. Korb, B. M. Gentry, and C. Y. Weng, "Edge Technique; Theory and Application to the Lidar Measurement of Atmospheric Wind", *Applied Optics*, **31**, 21, 4202-4213 (1992).
10. C. L. Korb, B. M. Gentry, and C. Y. Weng, "Spaceborne Lidar Wind Measurements with the Edge Technique", *Satellite Remote Sensing*, Rome, (1994).
11. I. L. Fabelinskii, *Molecular Scattering of Light*. (Plenum Press, New York, 1968).
12. R. Y. Chiao and B. P. Stoicheff, "Brillouin scattering in liquids excited by the He-Ne maser", *Journal of the Optical Society of America*, **54**, 1286-87 (1964).
13. G. B. Bendek, J. B. Lastovka, K. Fritsch, and T. Greytak, "Brillouin scattering in liquids and solids using low-power lasers", *Journal of the Optical Society of America*, **54**, 1284-85 (1964).
14. E. S. Fry, Q. Hu, and X. Li, "Single-Frequency Operation of an Injection-Seeded Nd:YAG Laser in High Noise and Vibration Environments", *Appl. Opt.*, **30**, 9, 1015-1017 (1990).
15. L. Bertotti, Y. Emery, C. Flesia, R. Miles, G. Galletti, and E. Zanzotera, "Incoherent Doppler wind Lidar Technologies", ESA/ESTEC 12789/94/NL/SB, (1995).

On Brillouin LIDAR Measurements of Oceanic Temperature and Sound Velocity

Edward S. Fry, Yves Emery, Xiaohong Quan, and Jeffrey W. Katz

Department of Physics, Texas A&M University

College Station, TX 77843

Texas Laser Laboratory, Houston Advanced Research Center

The Woodlands, TX 77381

Abstract

In this paper, we rigorously analyze Brillouin LIDAR measurements of the temperature and sound velocity. There are five variables: Brillouin shift, sound velocity, index of refraction, temperature and salinity and three well-known relations between them. In order to express all of them in terms of a single independent variable (e.g. Brillouin shift), one more relation is required. For the purpose of such a relation, the present study employs the mean value and standard deviation of salinity data obtained by analyzing a very large set of historical in-situ data. Temperature and sound velocity measurements can be expected down to 100 meters depth to have an accuracy as high as of 0.1 degree and 0.2 m/s, respectively.

Key words:

Brillouin, LIDAR, temperature, sound velocity, salinity variability, refractive index.

1. Introduction

Accurate remote sensing of the temperature and sound velocity structure of the upper-ocean mixed layers is of major importance to the understanding of the physical and biological behavior of the ocean.^{1, 2} There are also many other applications; it is, for example, a necessary input to weather forecast and climate change studies.³ There currently exists no instrumentation for remote sensing of these parameters, and only *in-situ* measurements have been performed with the required accuracy. However, *in-situ* approaches do not allow the rapid, accurate, and real-time range-resolved monitoring that is needed. LIDAR remote sensing provides a promising solution. Raman and Brillouin backscattering are both sensitive to temperature, and Brillouin scattering is directly related to sound velocity. Both processes have been previously considered for LIDAR measurements of the vertical structure of temperature and sound velocity in the ocean.²⁻¹³ Major relative limitations of the Raman method include: (1) The large Raman frequency shift, which means the transmitted laser field and/or the backscattered field must be in a relatively highly absorbing region of the water spectrum. (2) The Raman backscattering spectrum has a much wider frequency distribution than the Brillouin backscattering one. Consequently, the Raman receiver must have a much wider bandwidth and is therefore much more susceptible to background signals and noise.¹² As a result of these limitations, the Raman technique does not appear promising.

Several studies have shown the potential accuracy of LIDAR measurements of sound velocity and temperature in the ocean by

measuring the spectral shift of the backscattered Brillouin lines.^{2, 6, 8} Leonard and Sweeney¹² have even said that to achieve a temperature accuracy in the range of millidegrees over two or three attenuation lengths, advanced Brillouin methods must be invoked. However, taking into account other relevant factors, we show in this paper that for Brillouin measurements alone (i.e. no additional complementary measurements), the expected accuracy is only some tenths of a degree; this is however sufficient for many applications. Previously, technical limitations had prevented the realization of such Brillouin LIDAR instrumentation. Nevertheless the required technology, in particular pulsed lasers with a Fourier transform limited bandwidth, are now commercially available,² and a receiver based on an edge technique¹⁴ using absorption lines in Br₂ and I₂ now appears feasible.¹⁵ We emphasize that the objective of this paper is to determine general limits on the accuracy of LIDAR Brillouin shift measurements and not to describe an overall system.

The Brillouin lines consist of two inelastically scattered Lorentzians centered symmetrically at $\pm v_B$ with respect to the transmitted laser line; for water the FWHM of the Brillouin lines is approximately 0.5 GHz and v_B is 7 to 8 GHz. For a given incident laser wavelength λ , the relation between the Brillouin shift v_B and the velocity of sound v_s in ocean water is given for 180° backscattering by,^{1, 2}

$$v_B(S, T, p) = \frac{2n(S, T, \lambda)}{\lambda} v_s(S, T, p), \quad (1)$$

where n is the refractive index of water, S is the salinity, T is the temperature, and p is the pressure.

To derive the sound velocity from the Brillouin shift measurement, the refractive index n has frequently been assumed to be known.^{1, 8, 10} A more accurate approach had been considered by Hickman, *et al.*,² who point out that the uncertainty in our knowledge of the refractive index due to our uncertainty in T and S contributes to the error in the measurement of the sound velocity. Using an empirical relation for the refractive index as a function of T and S ,¹⁶ and assuming that T is known to $\pm 2^\circ\text{C}$, and S is known to $\pm 1\text{‰}$, they estimate that the refractive index variability limits the sound velocity accuracy to approximately 0.5 m/s.

To derive the temperature from the Brillouin shift measurement, an empirical equation is generally used to describe the dependence of the sound velocity on S , T , and p .¹⁷ Then using the measured Brillouin shift and assuming knowledge of the salinity, the refractive index, and the pressure, Eq. 1 gives the temperature.^{1, 10, 12}

In this paper, we will provide a rigorous approach to these interdependencies. We will identify five variables (v_B , S , T , v_s , n) and since we will have three relations between them, two of these variables must be independent, and three must be dependent. Since we will measure v_B , we take it as one of the independent variables. We take S as the other independent variable, and obtain empirical equations for the dependent variables T , v_s , and n as a function of the independent variables v_B and S . Such equations for T and v_s as a

function of v_B and S will be given in this paper. Throughout the discussion we will neglect the dependence on pressure since it is a well-known function of depth and can be included later.

Since S is the other independent variable, a very large set of *in-situ* salinity measurements was analyzed to determine the salinity mean value and standard deviation as a function of depth and location. These results enable us to determine a limit on the accuracy in the retrieval of T and v_s from measurements of the Brillouin shift, when historical data are used for the salinity mean value and standard deviation.

The relations between v_B , S , T , v_s and n are examined in Sect. 2. The limit on the accuracy of measurements of T and v_s are discussed in Sect. 3; effects due to the estimates of the variability in S and to the errors in the measurement of v_B are included.

2. Relations between Brillouin shift, salinity, temperature, and sound velocity in the ocean.

The most widely used empirical equation for the dependence of sound velocity on salinity, temperature, and pressure in natural water is given by:¹⁷

$$v_s(S, T, p) = c_0 + c_1 T + c_2 T^2 + c_3 T^3 + c_4 S + c_5 S^2 + c_6 TS + c_7 T^2 S + f(S, T, p), \quad (2)$$

where the coefficients c_i are constants and $f(S, T, p)$ represents all the terms containing the pressure. The c_i 's with T in $^{\circ}\text{C}$, S in ‰ , p in atm,

and v_s in m/sec are given in Table I. Typical values for the present application range between 0 °C and 30 °C for T , 0 ‰ (fresh water) and 40 ‰ for S , and 1 atm and 10 atm for p (corresponding to depths of 0 and approximately 100 meters, respectively). Typical values for the changes in v_s due to changes in p , T , and S are:

$$\begin{aligned} \left(\frac{\partial v_s}{\partial p} \right)_{S=35\text{‰}, T=10^\circ\text{C}, p=0} &= 0.16 \frac{\text{m/sec}}{\text{atm}}, \\ \left(\frac{\partial v_s}{\partial T} \right)_{S=35\text{‰}, T=10^\circ\text{C}, p=0} &= 3.5 \frac{\text{m/sec}}{^\circ\text{C}}, \text{ and} \\ \left(\frac{\partial v_s}{\partial S} \right)_{S=35\text{‰}, T=10^\circ\text{C}, p=0} &= 1.22 \frac{\text{m/sec}}{\text{‰}}. \end{aligned} \quad (3)$$

It should also be noted that the horizontal variability of pressure at a given depth is negligible. For simplicity, the pressure is assumed to be zero for the present calculations, i.e. $f(S, T, p) = 0$. Generalization to other pressures is straightforward.

An empirical equation for the dependence of the refractive index n of sea water at atmospheric pressure on temperature, salinity, and wavelength is given by:¹⁸

$$n(S, T, \lambda) = n_0 + S(n_1 + n_2 T + n_3 T^2) + n_4 T^2 + \frac{n_5 + n_6 S + n_7 T}{\lambda} + \frac{n_8}{\lambda^2} + \frac{n_9}{\lambda^3}, \quad (4)$$

where λ is the wavelength in nanometers, T is in °C, S is in ‰, and the coefficients n_j are constants, given in Table II.

Again, the five variables of interest are v_B , S , T , v_s , and n . Since Eqs. 1, 2, and 4 provide three relations between them, any two of the five can be chosen as independent. Our choices are v_B and S since the former is our measurement result, and the latter is the most stable and well-known, as we will see in section 3.1. With these two as independent variables, the other three variables can be expressed as $T(S, v_B)$, $v_s(S, v_B)$, and $n(S, v_B)$.

To obtain empirical equations for $T(S, v_B)$ and $v_s(S, v_B)$, we use Eqs. 1, 2, and 4 to generate a table containing $v_s(S, T)$, $n(S, T)$, and $v_B(S, T)$ at fixed values of S and T (Table III). Then, taking the entries for S , v_B , and T , a least-squares fit is performed to determine a function $T(S, v_B)$ of the form:

$$T(S, v_B) = t_0 + t_1(v_B - 7.5) + t_2(v_B - 7.5)^2 + t_3(v_B - 7.5)^3 + t_4(v_B - 7.5)^4 + S[t_5 + t_6(v_B - 7.5) + t_7(v_B - 7.5)^2 + t_8(v_B - 7.5)^3]. \quad (5)$$

The resulting t_j are given in Table IV. Numerical evaluations of Eq. 5 are shown in Fig. 1, where T is plotted as a function of S for various values of v_B (7.4 GHz to 7.7 GHz in steps of 50 MHz), and in Fig. 2, where T is plotted as a function of v_B for various values of S (30‰ to 40‰ in steps of 2.5‰).

Similarly, for the sound velocity, we use the entries for S , v_B , and v_s , to perform a least-squares fit and obtain a function $v_s(S, v_B)$ of the form:

$$v_s(S, v_B) = c'_0 + c'_1(v_B - 7.5) + c'_2(v_B - 7.5)^2 + c'_3(v_B - 7.5)^3 + S[c'_4 + c'_5(v_B - 7.5) + c'_6(v_B - 7.5)^2]. \quad (6)$$

The resulting c'_j are given in Table V. Numerical evaluations of Eq. 6 are shown in Fig. 3, where v_s is plotted as a function of S for v_B from 7.4 to 7.7 GHz in steps of 50 MHz, and in Fig. 4, where v_s is plotted as a function of v_B for S from 30‰ to 40‰ in steps of 5‰. Eqs. 5 and 6 together with the coefficients in Tables III and IV are valid for $30\text{‰} < S < 40\text{‰}$ and $7.0\text{ GHz} < v_B < 8.0\text{ GHz}$.

Fig. 1 shows that the temperature has a relatively weak dependence on the salinity. Specifically, from Eq. 5, we find

$$\left. \frac{\partial T}{\partial S} \right|_{v_B=7.5\text{GHz}} = t_s = -0.4 \text{ } ^\circ\text{C}/\text{‰}. \quad (7)$$

For example, if the uncertainty in the salinity is about 0.5‰, the uncertainty in the temperature measurement is $\leq 0.2 \text{ } ^\circ\text{C}$. We will see in section 3.1 that such an uncertainty in the salinity of this magnitude or less occurs frequently in historical data for salinity in the ocean at a given depth and location.

On the other hand, Fig. 2 shows a relatively strong dependence of T on v_B . From Eq. 5 we have

$$\left. \frac{\partial T}{\partial v_B} \right|_{S=35\text{‰}, v_B=7.5\text{GHz}} = t_1 + St_s = 0.056 \text{ } ^\circ\text{C}/\text{MHz}. \quad (8)$$

Uncertainties in Brillouin shift measurements of 1 MHz would lead to temperature uncertainties of about $0.06 \text{ } ^\circ\text{C}$. As will be discussed in section 3.2, such a measurement accuracy can be expected with a Brillouin LIDAR.

The weak dependence on the salinity is even more pronounced in the data of Fig. 3 for the sound velocity as a function of the salinity. Specifically, Eq. 6 gives

$$\left. \frac{\partial v_s}{\partial S} \right|_{v_B=7.5\text{GHz}} = c'_4 = -0.24 \text{ m/s / } \text{‰}; \quad (9)$$

thus an uncertainty in the salinity of 0.5‰ gives an uncertainty in the sound velocity of ≈ 0.12 m/s. Actually, a very rough knowledge of the salinity (a few ‰) is sufficient to determine the sound velocity with an uncertainty less than 1 m/s.

Fig. 4 shows that the dependence of v_s on v_B is relatively strong. Eq. 6 gives:

$$\left. \frac{\partial v_s}{\partial v_B} \right|_{S=35\text{‰}, v_B=7.5\text{GHz}} = c'_1 + S c'_5 = 0.2 \text{ m/s / MHz}. \quad (10)$$

Thus, a measurement error in the Brillouin shift of 1 MHz corresponds to an uncertainty of 0.2 m/s for the sound velocity.

Compared to previous studies, use of the three relations (Eqs. 1, 2, and 4) has enabled us to rephrase the problem so that only the uncertainties in v_B and S contribute; for example, temperature has become a derived quantity and its uncertainty is irrelevant to the determination of the uncertainty in v_s .

3. Measurement uncertainty in the temperature and sound velocity.

The root mean square error (uncertainty) in measurements of the temperature, δT , and sound velocity, δv_s , can be expressed in terms of the uncertainties in the salinity δS and Brillouin shift δv_B :

$$\delta T = \sqrt{\left(\frac{\partial T}{\partial S}\right)^2 [\delta S]^2 + \left(\frac{\partial T}{\partial v_B}\right)^2 [\delta v_B]^2}, \quad (11)$$

$$\delta v_s = \sqrt{\left(\frac{\partial v_s}{\partial S}\right)^2 [\delta S]^2 + \left(\frac{\partial v_s}{\partial v_B}\right)^2 [\delta v_B]^2}. \quad (12)$$

The following two sections discuss estimates for the uncertainty in the salinity and in the Brillouin shift measurement.

3.1 Variability of the salinity in the ocean.

A standard deviation δS for the salinity has been estimated by referring to the Oceanographic Station Profile Time Series.¹⁹ It provides a compilation of oceanographic data obtained from repetitive samples taken along various ocean sections and at fixed coordinates (oceanic weather stations) between 1900 and 1990. We have analyzed this data set for the salinity variability at 113 geographical locations, distributed over all the oceans of the earth (more than 75,000 measurements). Each location corresponds to an area of about 500×500 km². For each location we have computed the mean value and the standard deviation at various depths. A typical example is shown in Fig. 5 at 32°15' S 17°30' E, near the Cape of Good

Hope, at a depth of 10 meters, and in an area of $30 \times 100 \text{ km}^2$. The variability of the salinity is constant over a period of 25 years.

The results of our analysis are summarized in Fig. 6, where the cumulative distribution of the salinity standard deviation is shown for depths of 10 meters (Fig 6.a) and 100 meters (Fig 6.b). It is expressed as a fraction of the total number of locations. In particular, for a depth of 10 meters, 50% of the locations have a salinity standard deviation δS less than 0.5‰, and in 92% of the cases, δS is less than 1‰. For a depth of 100 meters, δS is less than 0.2 ‰ for 43% of the locations, and is less than 1‰ for 99% of the locations. As expected, the standard deviation generally decreases with depth.

Some locations exhibit seasonal variations, which could be taken into account in the reduction of δS . An example is shown in Fig. 7 for measurements performed in the middle of the North Pacific ($34^\circ 00' \text{ N}$ $164^\circ 00' \text{ E}$) at depths of 10 m, 50 m, and 100 m, in an area of $50 \times 50 \text{ km}^2$. For this location, δS would be significantly smaller if the seasonal trend is considered.

We have also noticed that for a given station, δS does not substantially change when increasing or decreasing the horizontal sampling area or when increasing the thickness of the water cell considered at a given depth. This shows that the salinity is fairly stable, and that historical data provide very useful salinity data that can be used to determine T and v_s from Brillouin shift measurements.

3.2. Brillouin shift measurement accuracy.

The use of injection locking techniques enable one to produce stable laser pulses having a Fourier transform limited bandwidth of approximately 50 MHz at a wavelength of 532 nm.^{20, 21} The linewidth of the pulsed laser, as well as its stability, are no longer a technical limitation for measurements of the Brillouin shift.

For a range-resolved measurement, a non-scanning high-resolution spectroscopic technique is needed. The so-called edge technique¹⁴ has been demonstrated to be a very powerful method for the measurement of small frequency changes in an atmospheric Doppler LIDAR application. Laboratory measurements²² have given wind velocity with an uncertainty of 0.25 m/s, corresponding to a frequency change of less than 470 kHz at 1064 nm. This is presently the most sensitive method to be demonstrated for small frequency shift LIDAR measurements.²³ Such a technique has been considered for oceanic Brillouin shift measurements using a laser wavelength of 532 nm.^{2, 10, 24}

In a recent study² the statistical uncertainty δv_B in the measurement of the Brillouin shift is calculated for various effective attenuation coefficients γ of water, assuming a single laser shot (500 mJ), a depth resolution of 1.1 meter, and known technical parameters. For $\gamma < 0.04 \text{ m}^{-1}$ one can expect δv_B to be less than 4 MHz for depths down to 100 meters, and less than 1 MHz for depths down to 75 meters. Based on these results, we consider two typical

Brillouin shift measurement errors δv_B of 1 MHz and 4 MHz in the following estimates.

3.3. Temperature and sound velocity measurement accuracy.

Eqs. 5 and 6 and the estimates of δS and δv_B made in the last two sections allow the evaluation of the temperature and sound velocity measurement errors given by Eqs. 11 and 12.

Fig. 8 shows the standard deviation in the temperature δT for $\delta S=0.5\text{‰}$ and $\delta v_B = 1$ MHz. This uncertainty δT is plotted as a function of S for typical oceanic values between 30‰ and 40‰, and with v_B as a parameter from 7.4 GHz to 7.7 GHz in steps of 50 MHz. For a typical value of $v_B=7.5$ GHz, the temperature resolution is about 0.2 °C.

Fig. 9 shows δT (left side y-axis) as a function of δS superposed on the cumulative distribution for the salinity standard deviation at a depth of 100 meters (right-side y-axis) as in Fig. 6b. For these results we have taken $v_B=7.5$ GHz and $S=35\text{‰}$. When δS is smaller than $\approx 0.3\text{‰}$, the uncertainty δv_B is the dominant contribution to δT . If δv_B is less than 1 MHz, the uncertainty in the temperature is less than 0.15 °C for more than 50 % of the locations. At 99% of the locations $\delta S < 1\text{‰}$, thus if $\delta v_B=4$ MHz, δT is less than 0.5 °C at these locations.

Fig. 10 shows the standard deviation of the sound velocity δv , for $\delta S=0.5\text{‰}$ and $\delta v_B=1$ MHz. This uncertainty δv , is plotted as a function of S for $30\text{‰} \leq S \leq 40\text{‰}$ and $7.4 \text{ GHz} \leq v_B \leq 7.7 \text{ GHz}$ in steps of 50

MHz. Notice that throughout the range of parameters for Fig. 10, the sound velocity uncertainty is always less than about 0.25 m/s.

Fig. 11 shows δv_s (left side y-axis) as a function of δS superposed on the cumulative distribution of the salinity standard deviation (right side y-axis) at a depth of 100 meters, as in Fig. 6b. For these results we have also taken $v_B=7.5$ GHz and $S=35\text{‰}$. The small slope of $\delta v_s(\delta S)$ is a consequence of the weak dependence of v_s on S . The Brillouin frequency shift is the dominant contribution to the uncertainty in a sound velocity measurement. Assuming δv_B is less than 1 MHz, δv_s is less than 0.3 m/s for more than 99% of the locations. Even for $\delta v_B=4$ MHz, δv_s is still always less than 1 m/s.

In fresh water there are only 4 parameters since S is already known to be zero. Since there are three relations, measurement of one parameter, v_B , is sufficient to determine the others. For the determination of the accuracy of Brillouin LIDAR measurements in fresh water, we set S and δS to 0. Then for $\delta v_B=1$ MHz, we find δT is about 0.06 °C, and δv_s is about 0.2 m/s.

Finally, it should be noted that if one more of the variables v_B , S , T , v_s , and n , or equivalently one more relation between them is also measured, then all the others, including salinity can be determined without the necessity of recourse to historical data for salinity. There are several possibilities, including simultaneous use of Raman scattering, or, for example, measurements of conductivity. For some situations there is also an S - T relationship²⁵ that may be applicable to increase the measurement accuracy.

4. Conclusions

We have obtained rigorous relations between v_B , S , T , v_s , and n , and have used them to determine the limits of accuracy of a Brillouin LIDAR system. We have also analyzed a large set of historical data to determine the mean and the standard deviation of the salinity. Use of this additional parameter allows us, to show that the temperature and sound velocity can be retrieved with an accuracy sufficient for many applications. Implementation of a Brillouin LIDAR system is underway, and the first frequency resolved measurement of the Brillouin lines using a pulsed laser have been recently obtained.¹⁵

5. Acknowledgments

The authors would like to thank George Kattawar, Thomas Walther, and Dan Hickman for many useful discussions. The work is supported by the Robert A. Welch Foundation Grant No. A-1218, the Texas Advanced Technology Program Grant 010366-16, the Office of Naval Research Grant No N00014-96-1-0410, and the Swiss National Foundation of Sciences.

References

1. Collins, D.J., Bell, J.A., Zaoni, R., McDermid, I.S., Breckinridge, J.B. and Sepulveda, C.A. *Recent Progress in the Measurement of Temperature and Salinity by Optical Scattering* 247-263 (Proc. SPIE, 1984).
2. Hickman, G.D., Harding, J.M., Carnes, M., Pressman, A., Kattawar, G.W. and Fry, E.S. *Aircraft Laser Sensing of Sound Velocity in Water: Brillouin Scattering, Remote Sens. Environ.* 36, 165-178 (1991).
3. Leonard, D.A. and Caputo, B. *Remote sensing of the ocean mixed-layer depth, Optical Engineering* 22, 288-91 (1983).
4. Chang, C.H. and Young, L.A. *Seawater Temperature Measurement from Raman Spectra* Avco Everett research Laboratory, Inc. ARPA Order No. 2194; Contract No. N62269-73-C-0073 (1972)
5. Chang, C.H., Young, L.A. and Leonard, D.A. *Remote Measurement of Fluid Temperature by Raman Scattered Radiation* U. S. Patent 3,986,775, filed (1974)
6. Hirschberg, J.G., Wouters, A.W., F. N. Cooke, J., Simon, K.M. and Byrne, J.D. *Laser Application to Measure Vertical Sea Temperature and Turbidity* NASA Report CR-139184 (1975)
7. Leonard, D.A., Caputo, B. and Hoge, F.E. *Remote Sensing of Subsurface Water Temperature by Raman Scattering, Appl. Opt.* 18, 1732-1745 (1979).

8. Guagliardo, J.L. and Dufilho, H.L. *Range Resolved Brillouin Scattering Using a Pulsed Laser*, *Rev. Sci. Instrum.* **51**, 79-81 (1980).
9. Leonard, D.A. and Caputo, B. *Raman LIDAR for the Remote Measurement of Subsurface Ocean Parameters* 1-277-280 (Proc. SPIE, 1984).
10. Hirschberg, J.G., Byrne, J.D., Wouters, A.W. and Boynton, G.C. *Speed of Sound and Temperature in the Ocean by Brillouin Scattering*, *Appl. Opt.* **23**, 2624-2628 (1984).
11. Hirschberg, J.G. and Byrne, J.D. *Rapid Underwater Ocean Measurements Using Brillouin Scattering* 1-270-276 (Proc. SPIE, 1984).
12. Leonard, D.A. and Sweeney, H.E. *Remote Sensing of Ocean Physical Properties: A Comparison of Raman and Brillouin Techniques* 407-414 (Proc. SPIE, 1988).
13. Leonard, D.A. and Sweeney, H.E. *A Comparison of Stimulated and Spontaneous Laser Radar Methods for the Remote Sensing of Ocean Physical Properties* 1-568-582 (Proc. SPIE, Orlando, FL, 1990).
14. Korb, C.L., Gentry, B.M. and Weng, C.Y. *Edge Technique; Theory and Application to the Lidar Measurement of Atmospheric Wind*, *Applied Optics* **31**, 4202-4213 (1992).
15. Emery, Y. and Fry, E.S. *Laboratory development of a LIDAR for measurements of sound velocity in the ocean using Brillouin scattering* (Proc. SPIE, Halifax, 1996).
16. Sager, G. *Zur Refraktion von Licht im Meerwasser*, *Beitr. Meeresk* **33**, 63-72 (1974).

17. Del Grosso, V.A. *New Equation for the Speed of Sound in Natural Waters (with Comparisons to Other Equations)*, J. Acoust. Soc. Am. 56, 1084-1091 (1974).
18. Quan, X. and Fry, E.S. *An Empirical Expression for the Index of Refraction of Sea Water*, Appl. Opt. 34, 3477-3480 (1995).
19. *Oceanographic Station Profile Time Series* (National Oceanographic Data Center (NODC), User Services Branch, NOAA/NESDIS E/OC21, Washington, D. C., 1993).
20. Henderson, S.W., Yuen, E.H. and Fry, E.S. *Fast Resonance-Detection Technique for Single-Frequency Operation of Injection-Seeded Nd-YAG Lasers*, Opt. Lett. 11, 715-717 (1986).
21. Fry, E.S., Hu, Q. and Li, X. *Single-Frequency Operation of an Injection-Seeded Nd:YAG Laser in High Noise and Vibration Environments*, Appl. Opt. 30, 1015-1017 (1990).
22. Korb, C.L., Gentry, B.M. and Weng, C.Y. *Spaceborne Lidar Wind Measurements with the Edge Technique* (Rome, 1994).
23. Bertotti, L., Emery, Y., Flesia, C., Miles, R., Galletti, G. and Zanzotera, E. *Incoherent Doppler wind Lidar Technologies* ESA/ESTEC 12789/94/NL/SB (1995)
24. Fry, E. *Brillouin LIDAR receiver based on edges of absorption lines of I₂ and Br₂* Texas A&M University, Internal report (1992)
25. Emery, W.J. *Global mass water summary and review*, Oceanologia Acta 9, 383-91 (1986).

Figure Captions

- Fig. 1. Temperature $T(\nu_B, S)$ shown as a function of salinity S with the Brillouin frequency shift ν_B as a parameter between 7.4 and 7.5 GHz in steps of 50 MHz.
- Fig. 2. Temperature $T(\nu_B, S)$ shown as a function of the Brillouin frequency shift ν_B for values of salinity S from 30 ‰ to 40 ‰ in steps of 2.5 ‰.
- Fig. 3. Sound velocity, $v_s(\nu_B, S)$, shown as a function of salinity S with the Brillouin frequency shift ν_B as a parameter (in steps of 50 MHz).
- Fig. 4. Sound velocity, $v_s(\nu_B, S)$, shown as a function of the Brillouin frequency shift ν_B for values of salinity S from 30 ‰ to 40 ‰ in steps of 5 ‰.
- Fig. 5. Variability of the salinity at 32°15' S 17°30' E, in the South Atlantic, near the Cape of Good Hope, at a depth of 10 meters. Sampling area: 30×100 km².
- Fig. 6. Cumulative histogram of the variability of the salinity standard deviation for 113 locations for a depth of 10 meters (6a) and 100 meters (6b).

Fig. 7. Seasonal variability of the salinity at 34°00' N 164°00' E, in the middle of the North Pacific, at a depths of 10 m, 50 m, and 100 m. Sampling area: 50×50 km². The standard deviation represents the overall variability; the seasonal trend is not taken into account in the calculation.

Fig. 8. The uncertainty, δT , in the determination of temperature as a function of the salinity for $\delta S=0.5\text{‰}$ and $\delta \nu_B=1$ MHz, and various Brillouin shifts from 7.4 to 7.7 GHz in steps of 50 MHz.

Fig. 9. On the left-side y-axis, the uncertainty, δT , in the determination of temperature is plotted as a function of the salinity standard deviation, for $\delta \nu_B=1$ MHz (solid lines) and $\delta \nu_B=4$ MHz (dotted lines). In both cases we have taken $\nu_B=7.5$ GHz and $S=35 \text{‰}$. It is superposed on the salinity standard deviation cumulative probability distribution at 100 meters, on the right-side y-axis (same as Fig. 6b).

Fig. 10. The uncertainty $\delta \nu_S$ in the determination of sound speed as a function of salinity with ν_B as a parameter that is varied from 7.4 GHz to 7.7 GHz in

steps of 50 MHz. For these calculations we have taken $\delta v_B = 1$ MHz and $S = 0.5\%$.

Fig. 11 On the left-side y-axis, the uncertainty, δv_s , in the determination of sound velocity is plotted as a function of the salinity standard deviation, for $\delta v_B = 1$ MHz (solid lines) and $\delta v_B = 4$ MHz (dotted lines). In both cases we have taken $v_B = 7.5$ GHz and $S = 35\%$. It is superposed on the salinity standard deviation cumulative probability distribution at 100 meters, on the right-side y-axis (same as Fig. 6b).

Tables

Table I. Coefficients in the empirical expression for the sound velocity $v_s(S,T)$.¹⁷

$c_0=1402.392$	$c_1=5.01109398873,$
$c_2=-0.0550946843172$	$c_3=0.00022153596924,$
$c_4=1.32952290781$	$c_5=0.0001289557568,$
$c_6=-0.0127562783426$	$c_7=0.000096840315641.$

Table II. Coefficients in the empirical expression for the refractive index $n(S,T,\lambda)$.¹⁸

$n_0=1.31405,$	$n_1=1.779 \times 10^{-4},$	$n_2=-1.05 \times 10^{-6},$
$n_3=1.6 \times 10^{-8},$	$n_4=-2.02 \times 10^{-6},$	$n_5=15.868,$
$n_6=0.01155,$	$n_7=-0.00423,$	$n_8=-4382,$
	$n_9=1.1455 \times 10^6.$	

Table III. n , v_s [m/s], v_B [GHz], for a range of values of $30‰ < S < 40‰$ and $0^\circ\text{C} < T < 40^\circ\text{C}$;
 $p=0$ atm, and $\lambda=532.57$ nm.

S	30			32.5			35.0			37.5			40.0		
	n	v_s	v_B	n	v_s	v_B	n	v_s	v_B	n	v_s	v_B	n	v_s	v_B
0	1.34197	1442.39	7.26907	1.34247	1445.74	7.28863	1.34296	1449.08	7.30821	1.34346	1452.43	7.32781	1.34396	1455.78	7.34744
5	1.34173	1464.26	7.37796	1.34222	1467.45	7.39672	1.34270	1470.64	7.41550	1.34319	1473.84	7.43430	1.34368	1477.03	7.45312
10	1.34142	1483.68	7.47408	1.34189	1486.73	7.49210	1.34237	1489.78	7.51014	1.34285	1492.83	7.52821	1.34332	1495.89	7.54628
15	1.34103	1500.82	7.55825	1.34189	1503.74	7.57560	1.34197	1506.67	7.59297	1.34243	1509.59	7.61036	1.34290	1512.51	7.62777
20	1.34156	1515.86	7.63130	1.34150	1518.66	7.64805	1.34149	1521.47	7.66482	1.34195	1524.27	7.68160	1.34241	1527.08	7.69840
25	1.34002	1528.95	7.69407	1.34048	1531.64	7.71029	1.34093	1534.34	7.72652	1.34139	1537.05	7.74277	1.34185	1539.75	7.75903
30	1.33940	1540.26	7.74740	1.34985	1542.86	7.76314	1.34031	1545.47	7.77891	1.34077	1548.08	7.79469	1.34122	1550.69	7.81049
35	1.33870	1549.95	7.79211	1.33916	1552.48	7.80746	1.33961	1555.00	7.82283	1.34007	1557.53	7.83821	1.34052	1560.06	7.85361
40	1.33792	1558.21	7.82906	1.33838	1560.66	7.84408	1.33884	1563.12	7.85912	1.33930	1565.58	7.87418	1.33976	1568.04	7.88925

Table IV. Coefficients in the empirical expression for $T(S, \nu_B)$
at 532.57 nm.

$t_0=23.689$	$t_1=68.696$	$t_2=51.939$
$t_3=225.809$	$t_4=274.492$	$t_5=-0.40554$
$t_6=-0.35856$	$t_7=-0.56583$	$t_8=-5.4252$

Table V. Coefficients in the empirical expression for $\nu_s(S, \nu_B)$
at 532.57 nm.

$c'_0=1496.17$	$c'_1=205.08$	$c'_2=30.924$
$c'_3=35.242$	$c'_4=-0.2406$	$c'_5=-0.08531$
	$c'_6=-0.6336$	

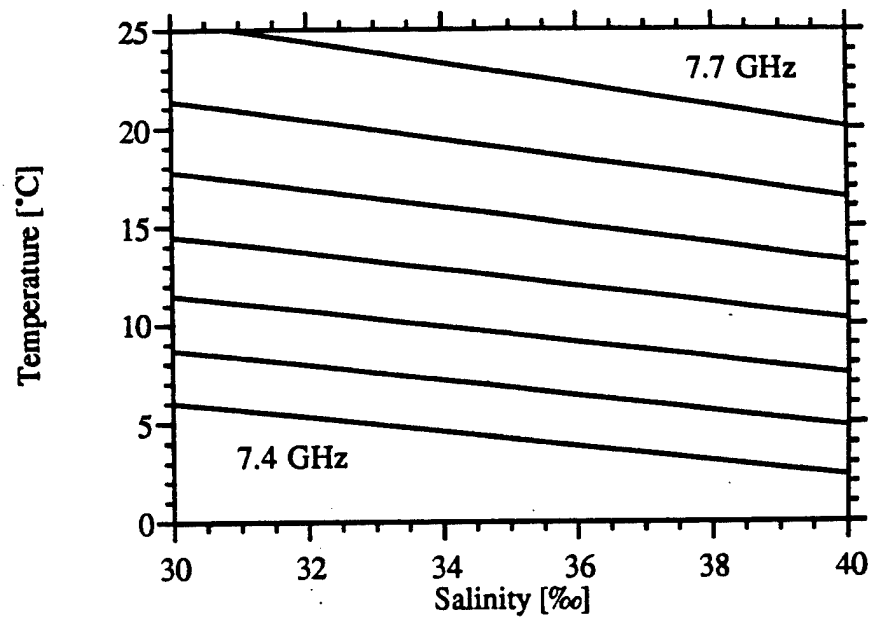


Fig. 1. Temperature $T(\nu_B, S)$ shown as a function of salinity S with the Brillouin frequency shift ν_B as a parameter between 7.4 and 7.5 GHz in steps of 50 MHz.

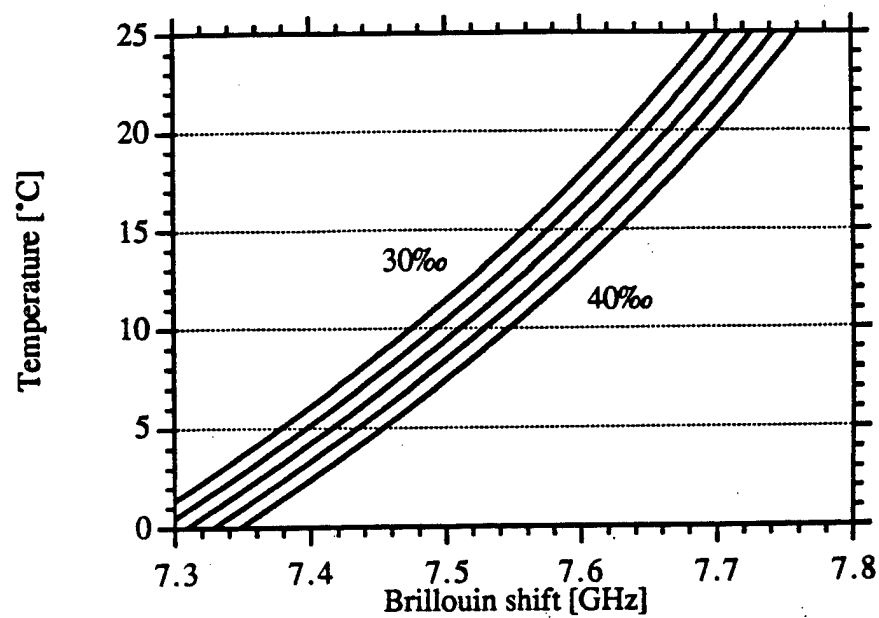


Fig. 2. Temperature $T(\nu_B, S)$ shown as a function of the Brillouin frequency shift ν_B for values of salinity S from 30 ‰ to 40 ‰ in steps of 2.5 ‰.

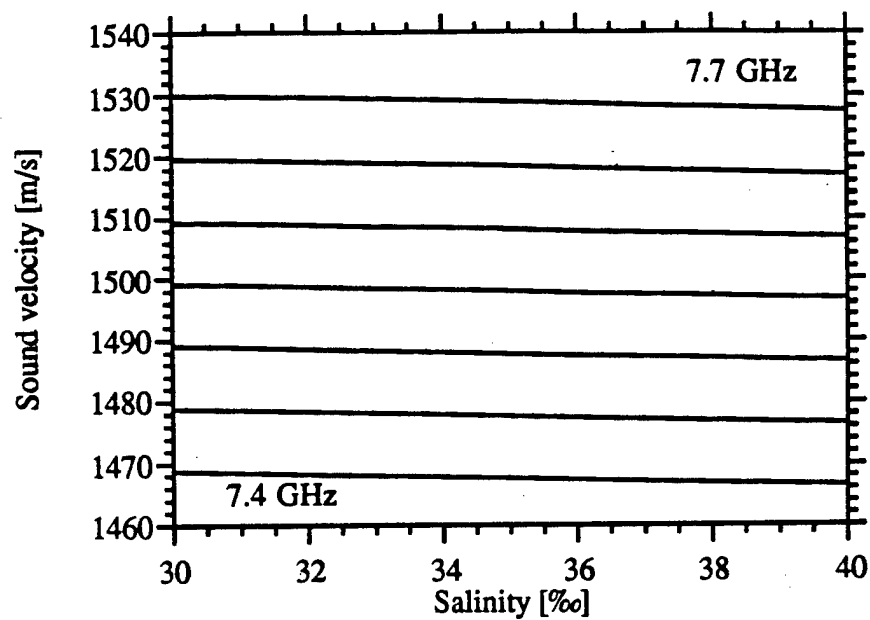


Fig. 3. Sound velocity, $v_s(v_B, S)$, shown as a function of salinity S with the Brillouin frequency shift v_B as a parameter (in steps of 50 MHz).

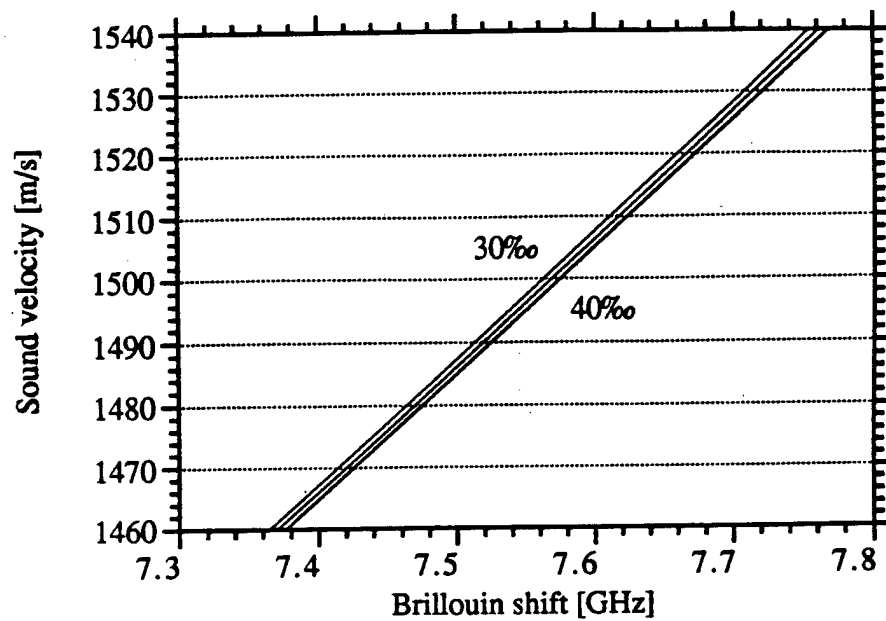


Fig. 4. Sound velocity, $v_s(v_B, S)$, shown as a function of the Brillouin frequency shift v_B for values of salinity S from 30 ‰ to 40 ‰ in steps of 5 ‰.

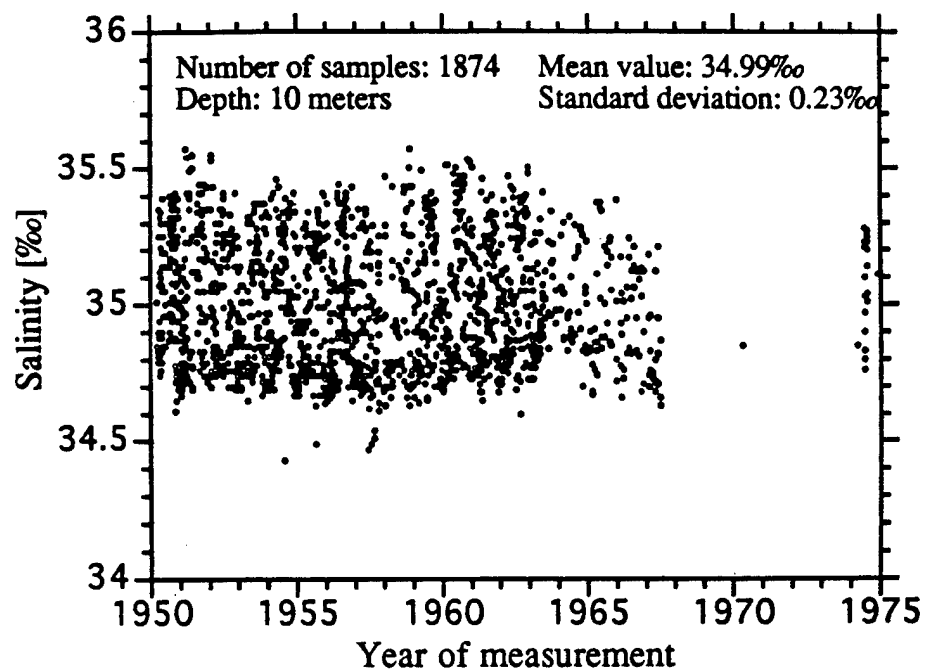


Fig. 5. Variability of the salinity at 32°15' S 17°30' E, in the South Atlantic, near the Cape of Good Hope, at a depth of 10 meters. Sampling area: 30×100 km².

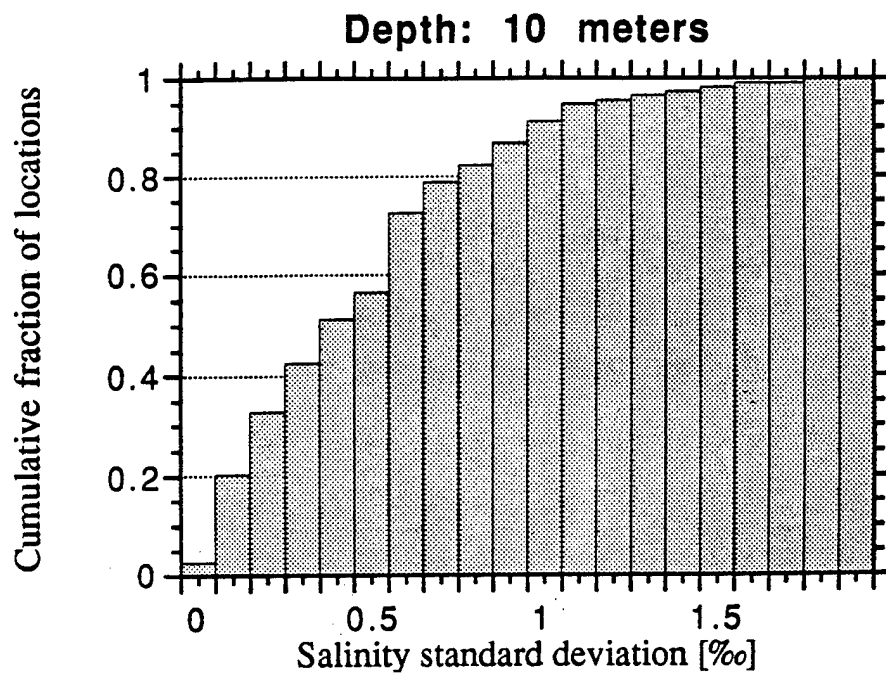


Fig. 6a. Cumulative histogram of the variability of the salinity standard deviation for 113 locations for a depth of 10 meters.

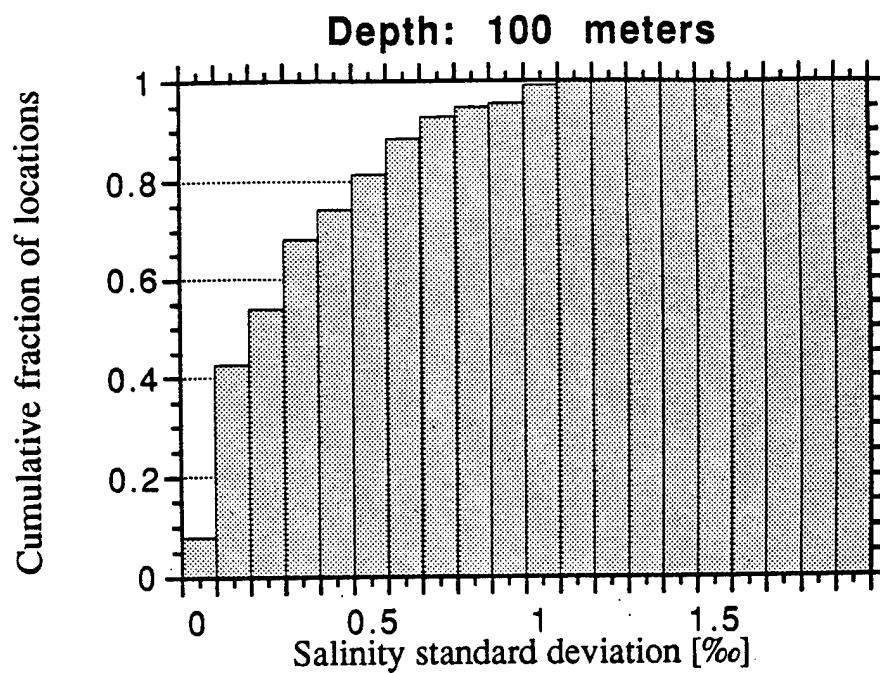


Fig. 6b. Cumulative histogram of the variability of the salinity standard deviation for 113 locations for a depth of 100 meters.

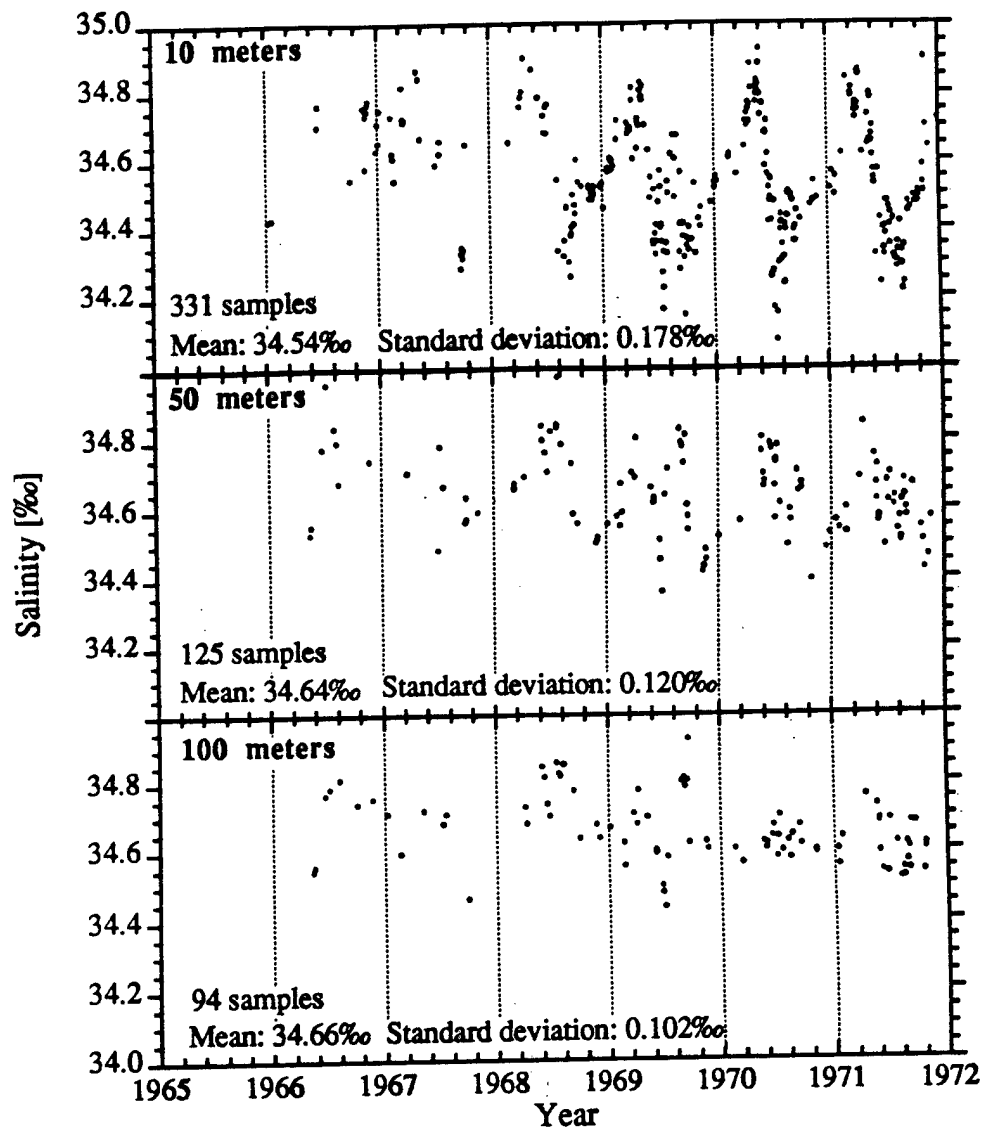


Fig. 7. Seasonal variability of the salinity at 34°00' N 164°00' E, in the middle of the North Pacific, at a depths of 10 m, 50 m, and 100 m. Sampling area: 50×50 km². The standard deviation represents the overall variability; the seasonal trend is not taken into account in the calculation.

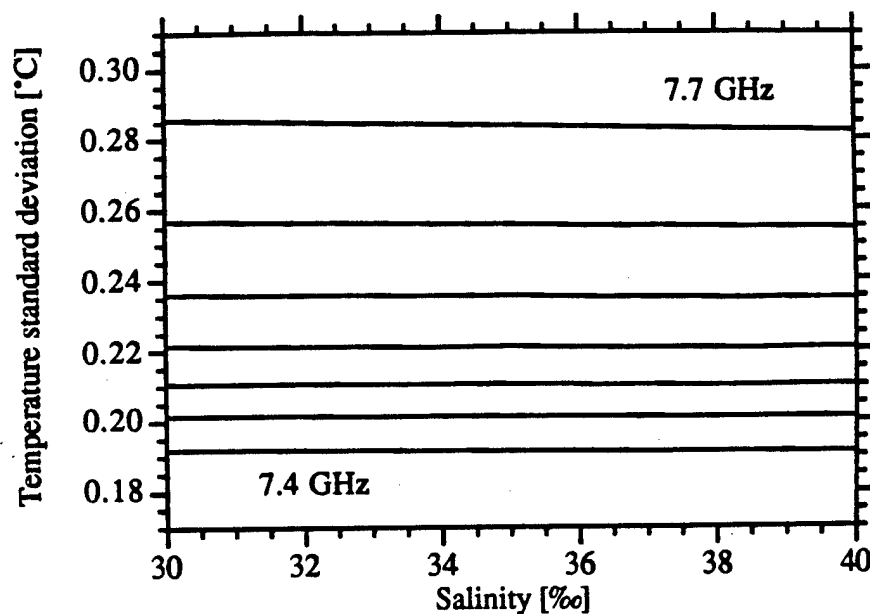


Fig. 8. The uncertainty, δT , in the determination of temperature as a function of the salinity for $\delta S=0.5\text{‰}$ and $\delta \nu_B=1\text{ MHz}$, and various Brillouin shifts from 7.4 to 7.7 GHz in steps of 50 MHz.

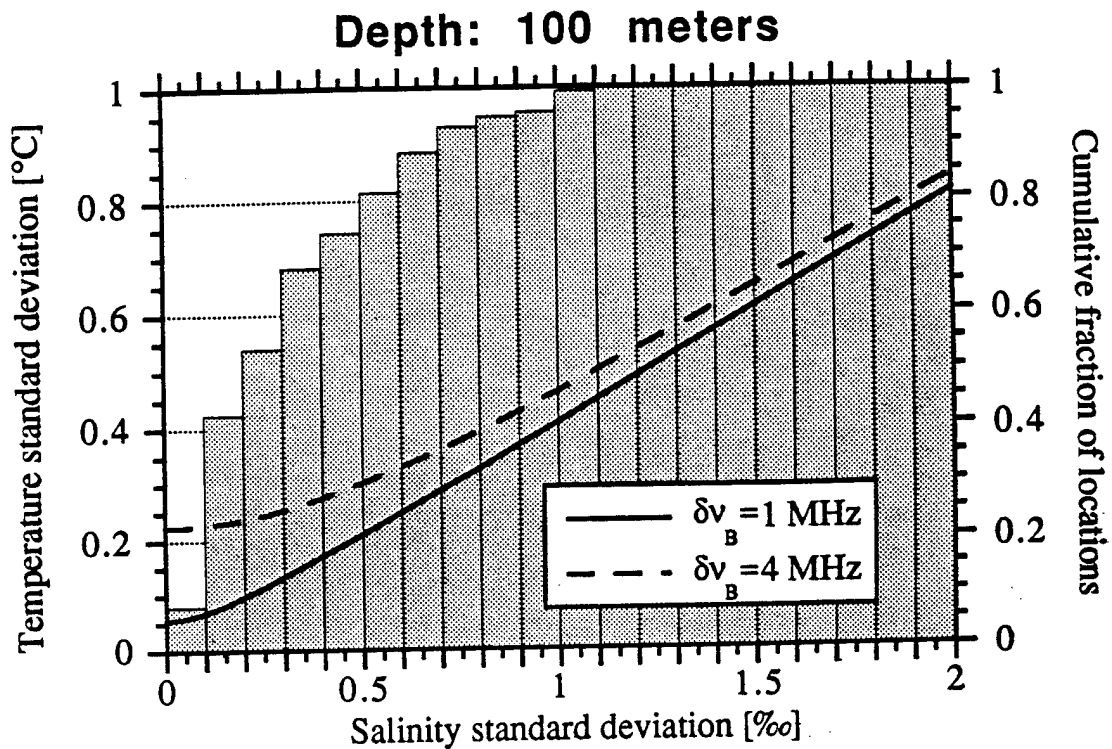


Fig. 9. On the left-side y-axis, the uncertainty, δT , in the determination of temperature is plotted as a function of the salinity standard deviation, for $\delta v_B = 1 \text{ MHz}$ (solid lines) and $\delta v_B = 4 \text{ MHz}$ (dotted lines). In both cases we have taken $v_B = 7.5 \text{ GHz}$ and $S = 35\text{‰}$. It is superposed on the salinity standard deviation cumulative probability distribution at 100 meters, on the right-side y-axis (same as Fig. 6b).

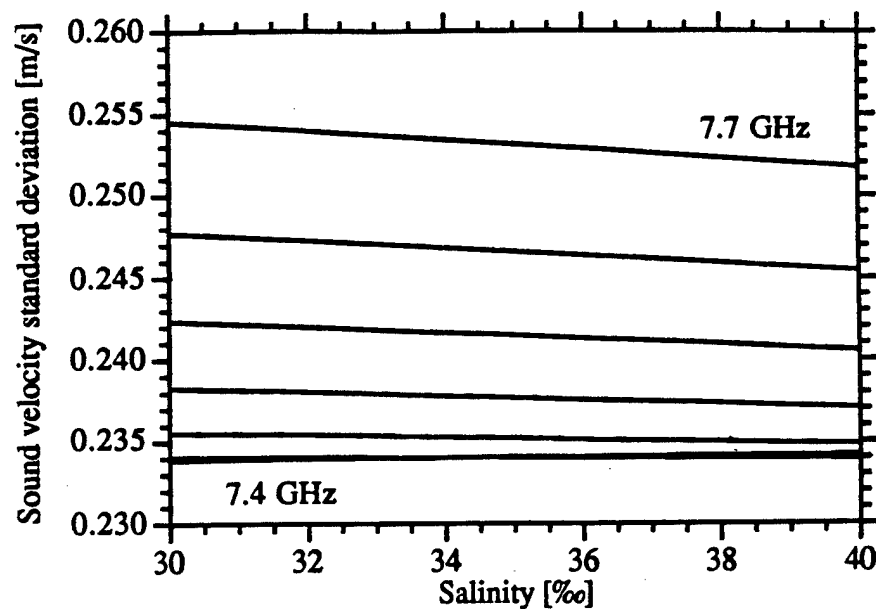


Fig. 10 The uncertainty δv_s in the determination of sound speed as a function of salinity with v_B as a parameter that is varied from 7.4 GHz to 7.7 GHz in steps of 50 MHz. For these calculations we have taken $\delta v_B = 1$ MHz and $\delta S = 0.5\text{‰}$.

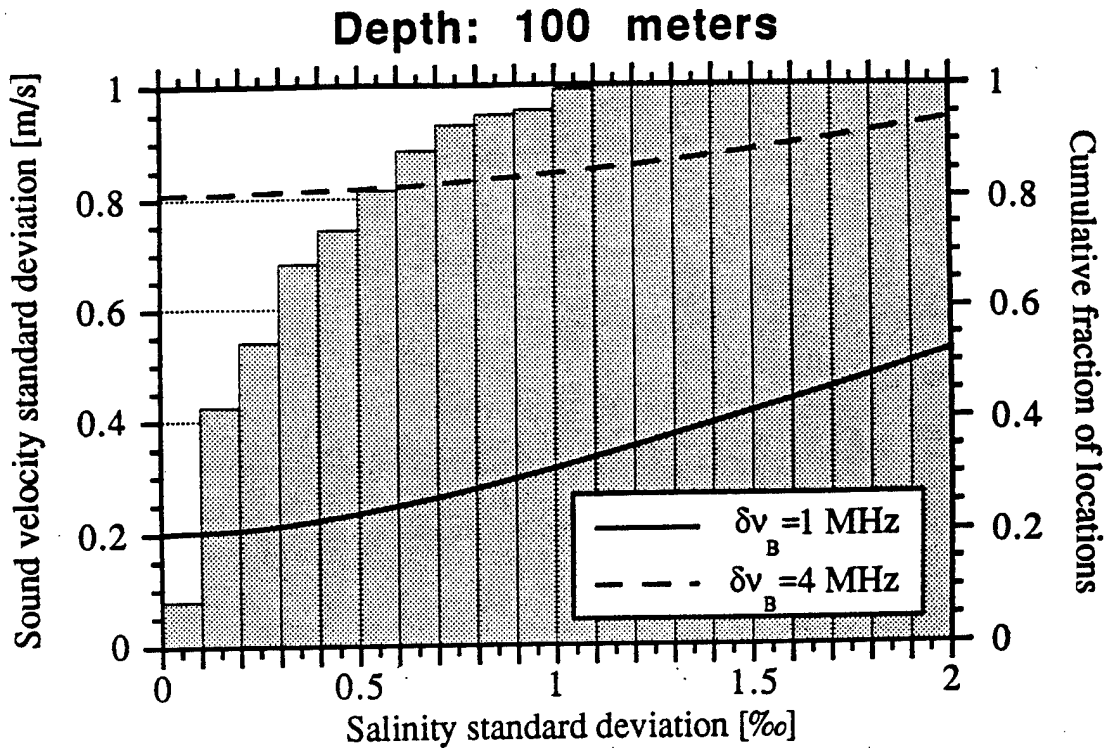


Fig. 11 On the left-side y-axis, the uncertainty, δv_s , in the determination of sound velocity is plotted as a function of the salinity standard deviation, for $\delta v_B = 1 \text{ MHz}$ (solid lines) and $\delta v_B = 4 \text{ MHz}$ (dotted lines). In both cases we have taken $v_B = 7.5 \text{ GHz}$ and $S = 35\text{‰}$. It is superposed on the salinity standard deviation cumulative probability distribution at 100 meters, on the right-side y-axis (same as Fig. 6b).